# Numerical Investigation of the Effect of Self-Dilution in Confined Turbulent Non-Premixed Flames on NOx Reduction

K.D.Kunkuma Amila Somarathne and Susumu Noda
Toyohashi University of Technology
Toyohashi, Aichi, Japan

## 1 Introduction

The control of nitrogen oxides (NOx) is currently a major issue in designing an effective combustion system because NOx has several detrimental effects on environment and human health. Nevertheless, non-premixed combustion, which is used in numerous industrial applications such as gas turbine, industrial furnaces, and internal combustion engines, suffers from a major problem on control of the NOx emission [1]. Because the chemical reactions proceed at the stoichiometric conditions, and thereby the flame temperature may exceed 1800 K, at which the thermal NO reactions are activated. Therefore, several combustion techniques have been proposed to reduce the NOx emission, including multistage combustion and flue gas recirculation combustion [2]. The flue gas recirculation technique is widely used in many practical applications. In this method, the combustion mixture is diluted by burnt gases, and hence, the dilution increases the heat capacity of the mixture of combustion chamber, which in turn, decreases the maximum temperature of combustion chamber, and thereby, thermal NO [3].

However, self-recirculation of burnt gases naturally takes place in a confined combustion system because of the wall confinement. In confined jet flames, a limited supply of surrounding fluids induces the formation of the recirculation vortex between the jet and furnace wall, and thereby confined jet flows undergo the entrainment of recirculated fluid at jet boundaries. The recirculation transports high-temperature burnt gases upstream, and introduces a mixing process that is related to flame stabilization and dilution [4]. A comprehensive investigation of the EINOx characteristics, which is defined as the ratio of the total grams of NOx produced to fuel 1kg burnt, of turbulent non-premixed flames in cylindrical furnaces was conducted by Noda et al. [5, 6], and illustrated that EINOx is significantly decreased by increasing the inner diameter of the furnace, turbulence at the flame boundary, and global equivalence ratio. This decrease of EINOx is possibly related to the self-dilution of combustion mixtures by burnt gases and flame stretch effect [5, 6].

In this study, calculations of these physical interactions are performed numerically on the basis of mathematical models. The computational evaluation quantifies the self-dilution in confined furnaces in terms of the inner diameter, and expresses the generalized idea about the NOx reduction by self-dilution in confined combustion systems.

Correspondence to: noda@me.tut.ac.jp 

## 2 Turbulent and Combustion Models

In this study, the flow calculation software OpenFOAM [7], which is a high-fidelity open source code, is employed as a finite-volume solver for Reynolds-Averaged Navier Stokes (RANS) equations on an unstructured mesh of cylindrical coordinate systems. The RANS equations include the conservation of mass of species, momentum, and sensible enthalpy. The $k-\omega$ SST model [8] is employed as a turbulent model. The OpenFOAM-reactingFOAM code solves these conservation and transport equations with a partially-stirred-reactor (PaSR) turbulent combustion model [9].

## 3 Chemical Kinetic Model and *In-Situ* Adaptive Tabulation

This study considers a detailed finite-rate chemistry model because the dilution of reactants with recirculation fluids slows down the chemistry; thereby fast chemistry assumption is not valid. Our previous study [10] verified that global kinetic models show the overprediction of temperature in the turbulent non-premixed combustion modeling using the PaSR model. Djavdan et al. [11] proposed and validated an argumented-starting mechanism for propane-air combustion, which includes 28-species and 69-elementray reaction steps. This was compared with the detailed propane-air chemical kinetic model of Warnatz, which involves 32-species and 123-reaction steps .The 28-species/69-steps kinetics showed a good agreement with Warnatz mechanism with a fair degree of precision [11], and was also computationally less expensive. Thus, in this study, the Djavdan propane-air mechanism was selected to use in PaSR model. However, the use of detailed chemistry model has become a burden in terms of computational cost. An *in-situ* adaptive tabulation (ISAT) algorithm library [12] is used to calculate the composition change due to the chemical reaction, and thereby reduce the computational burden.

## 4 NOx Modeling

There have been several studies [13-14] on NOx formation. In hydrocarbon flames, thermal and prompt mechanisms are the main routes for NOx formation. Hewson et al. [13] showed that when flame-residence times are short, and peak temperature is reduced, nitric-oxide production is minimized, and then the prompt mechanism becomes the dominant route for the formation of NOx. In addition, the study illustrated that NOx reburning chemistry is significant in flames, and the neglect of the prompt and reburning NOx chemistries leads to the underprediction of NOx emission for short residence time and overprediction for long residence time, respectively. Ju et al. [14] demonstrated that the prompt and thermal mechanisms are strongly coupled, and the decoupled mechanisms considerably overpredict the thermal NO and underpredicts the prompt NO. Therefore, this study employs the detailed NOx formation mechanism extracted from GRI 2.11 [15].

## 5 Numerical Conditions

Axisymmetric vertical furnaces consist of a burner in the cylindrical combustion chamber [5, 6]. The burner, which consists of a fuel nozzle surrounded by two air coaxial nozzles, is located at the center of the bottom of the furnace. The exit of the central fuel nozzle with an inner diameter of 2 mm, having a coaxial pilot nozzle of 0.4 mm annulus, is located 27 mm downstream of the furnace base. The chambers of the inner diameters of 95 mm and 182 mm, respectively, are 840 mm in height. The furnace exit is contracted to 38 mm in diameter. The high and low speed air nozzle annuluses are 4 mm and 8 mm, respectively. The propane-main-fuel and hydrogen-pilot-fuel inlet-velocities were set to 10.4 m/s and 4 m/s, respectively. The total air flow rate was fixed to 0.002 $m^3/s$. The high and low air velocities were 9.8 m/s and 1.8 m/s, respectively, and the velocity difference controls turbulence at the flame boundary. The global equivalence ratio is 0.4. The furnace walls are non-slip and adiabatic, and the furnace exit is specified by the continuity boundary conditions. The origin of the coordinates was set at the center of the fuel nozzle exit, and the axial and radial coordinates are indicated by z and r, respectively. The computational predictions are extensively compared with experimental measurements [5, 6].

# 6 Results and Discussion

**Flow Field:**

The radial distributions of the mean axial velocities at axial distance z = 25 mm through 200 mm in terms of the inner diameter of furnace, *D*, are shown together with the experimental measurements in Fig. 1. Negative axial velocities near the furnace wall in Fig. 1 clearly indicate the existence of recirculation vortices. Therefore, the flow field consists of two zones: jet-like propagation zone and recirculation zone. Moreover, Fig. 2 shows the vector maps of flow fields in combustion chambers up to z = 300 mm in terms of *D*, and shows a vortex generated between the fuel jet boundary and wall. The vector maps illustrate that, in the case of *D* = 95 mm, the recirculation exists until z = 270 mm. On the other hand, in the case of *D* = 182 mm, the recirculation exists beyond z = 300 mm. Recirculation vortex cores for *D* = 95 mm and 182 mm are located at the axial distance of z = 130 mm and 180 mm, respectively. This means that the recirculation vortex become larger with the increase in *D*.

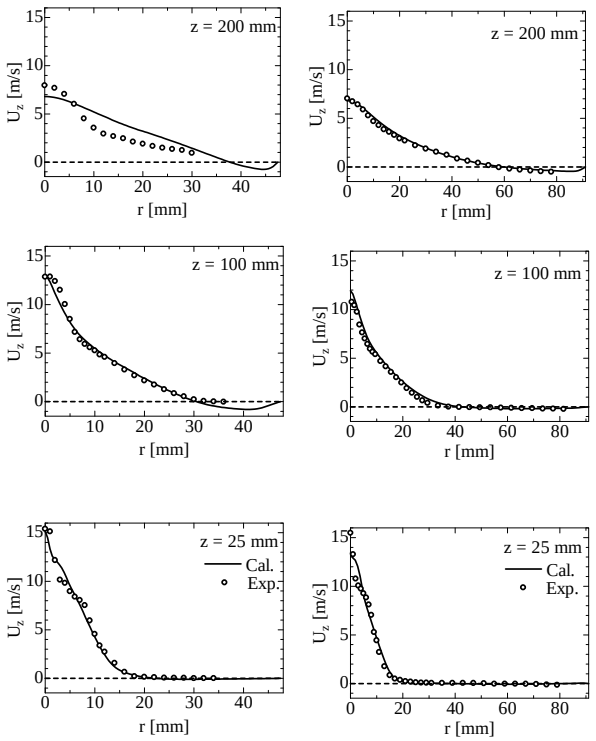


(a) *D* = 95 mm (b) *D* = 182 mm

Figure 1. Radial distributions of mean axial velocity, $U_z$, in terms of the *D*.

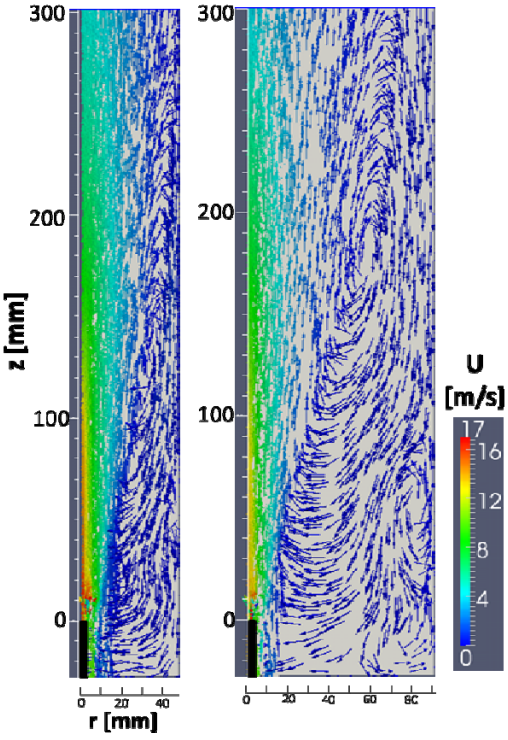


(a) *D* = 95 mm (b) *D* = 182 mm

Figure 2. Vector maps of flow fields in the combustion chambers in terms of *D*.

**Entrainment Characteristics:**

The recirculation flow characteristics are here discussed by examining the jet zone. To facilitate the discussion, a parameter that represents the mass flow rate of jet zone, $M_z$, is introduced:

$$M_z = \int_0^R 2\pi r \overline{\rho} \widetilde{U}_z dr \,, \tag{1}$$

where *R* is the maximum radius of the jet zone at each cross section, and $\rho$ is the density of combustion mixture. The bar and tilde denote an ensemble-averaged and a Favre-averaged values, respectively. Figure 3 shows the variation of $M_z$ along the axial direction in terms of the inner diameter, *D*. The $M_z$ increases in the upstream of the recirculation vortex because of the entrainment process, and decreases in the downstream of the vortex because of the discharge of gases from jet zone to recirculation zone. Therefore, the peak is located on the cross section of the core of the recirculation

vortex. Figure 3 illustrates that the increase in *D* enhances the entrainment process, and make a higher peak value of $M_z$. The entrainment factor, as defined in Eq. (2), characterizes the entrained mass quantity with respect to the jet zone mass flow rate, $M_z$.

$$\text{Entrainment Factor} = \frac{M_z - M_0}{M_z} \times 100, \tag{2}$$

where $M_0$ denotes the jet zone mass flow rate at z = 0 mm. The variation of entrainment characteristics are shown in Fig. 4 in terms of *D*. In the case of *D* = 95 mm, the maximum entrainment factor is 30%, whereas in *D* = 182 mm the maximum factor is about 49%. The enhancement of entrainment should lead to greater dilution of the flame.

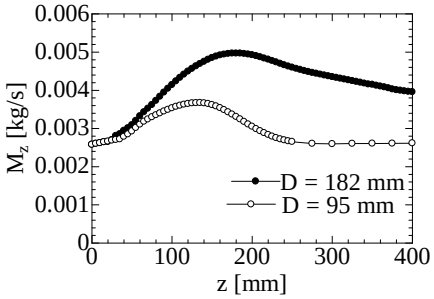


Figure 3. Jet zone mass flow rate, $M_z$, in terms of *D*

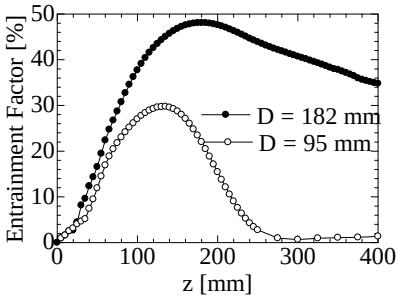


Figure 4. Entrainment factor in terms of *D*

**Dilution Characteristics:**

The entrainment of burnt and inert gases such as $CO_2$, $H_2O$, and $N_2$ into the flame, because of recirculation, leads to the dilution. The local dilution factor, as defined in Eq. (3), characterizes the entrained burnt and inert gases mass quantities in the flame at each cross section with the respect to the jet zone mass flow rate.

$$\text{Local Dilution Factor (z)} = \frac{\int_0^{\Delta z} \left[\frac{dM_z}{dz}\right] \times \left(\tilde{Y}_{CO2} + \tilde{Y}_{H2O} + \tilde{Y}_{N2}\right)_{Near\ wall}\ dz}{M_z} \times 100\ , \tag{3}$$

where *Y* is mass fraction of the species and Δz = 0.005 m.

Figure 5 shows the local dilution factor variation in terms of *D*. The increase in *D* increases the local dilution of the flame as shown in Fig. 5. The total flame dilution can be obtained by integrating local dilution factor along the axial direction as shown in Eq. (4).

$$\text{Total Flame Dilution} = \frac{\int_0^{z_1} \left[\frac{dM_z}{dz}\right] \times \tilde{Y}_{(CO_2+H_2O+N_2)\,Near\ wall}\,(z)\,dz}{M_{z,\max}} \times 100\ , \tag{4}$$

where $z_1$ locates the axial distance which has maximum jet zone mass flow rate, $M_{z,max}$. Thus, total flame dilution for *D* = 95 mm and 182 mm is 23% and 37%, respectively. The calculation verifies that total flame dilution is enhanced by the increase in inner diameter of the furnace.

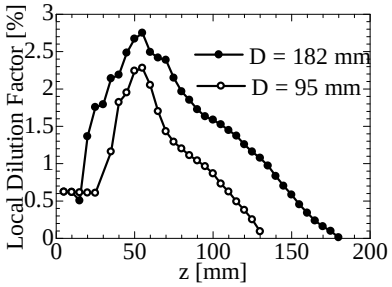


Figure 5. Local dilution factor variation in terms of the inner diameter, *D*.

**Temperature Characteristics:**

Figures 6 and 7 show variations in radial and axial temperatures, respectively, in terms of inner diameter of the furnace, *D*. The increase in *D* decreases the maximum temperature about 100 K in flame region. This is caused by the dilution through the strengthened burnt gases entrainment, resulting from the enlarged vortices. The increase in dilution increases the heat capacity of combustion mixture, and leads to the decrease of the flame temperature.

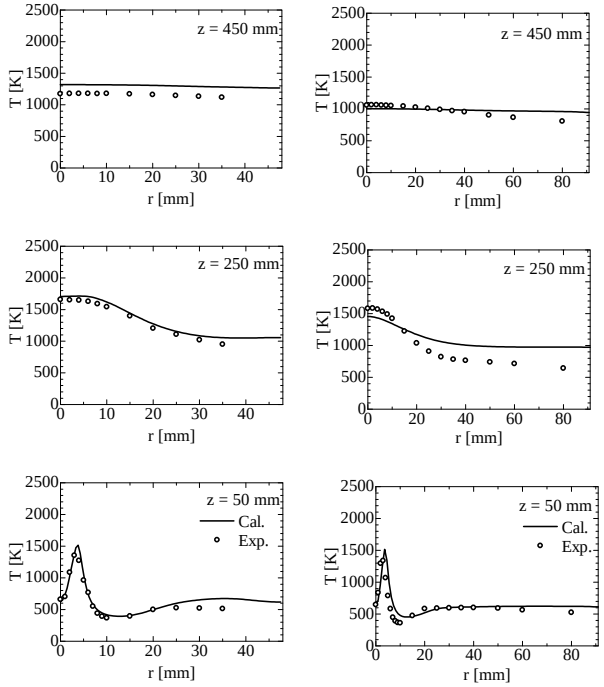


(a) *D* = 95 mm (b) *D* = 182 mm

Figure 6. Radial distribution of temperature in terms of *D*

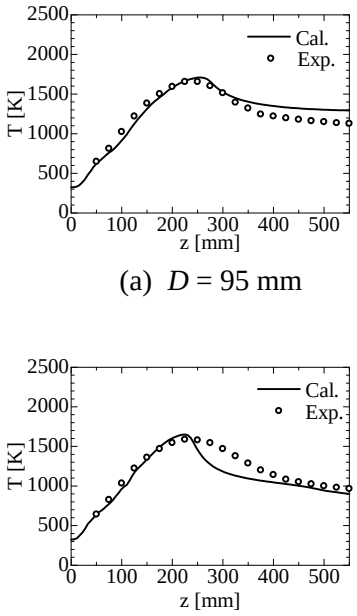


(a) *D* = 95 mm

(b) *D* = 182 mm

Figure 7. Axial distribution of temperature in terms of *D*

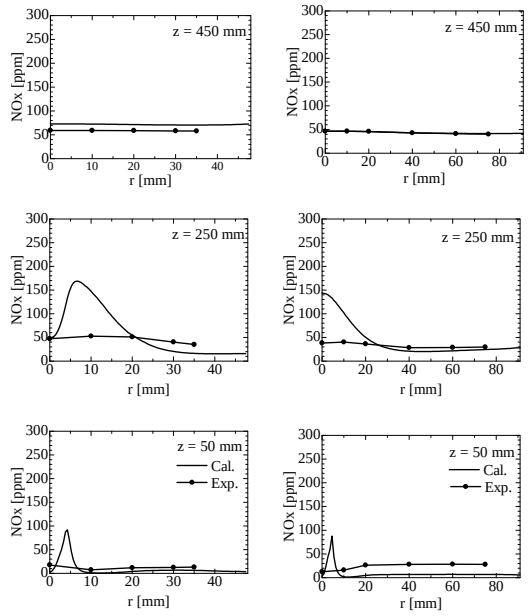


(a) *D* = 95 mm (b) *D* = 182 mm

Figure 8. Radial distribution of NOx emission in terms of *D*

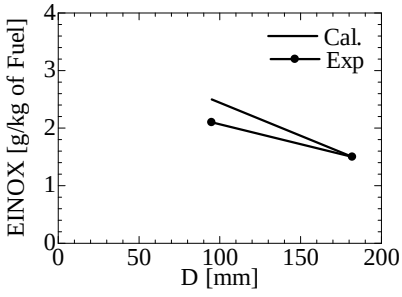


Figure 9. EINOx in terms of *D*

**NOx Emission Characteristics:**

Figure 8 shows NOx emission with respect to the inner diameter of the furnace, *D*. The NOx discrepancies at reaction zones of 50 mm and 250 mm between predictions and measurements may be caused by measurement errors, because NOx must increase in high temperature regions. The EINOx at the furnace exit was calculated by assuming the continuity of mass flow rate at the furnace exit, and is shown in Fig. 9. The increase in *D* decreases the EINOx. This is caused by the dilution, which in turn, decreases the maximum flame temperature, and thereby, thermal NO. Then, CO increased slightly in the concentration less than 300 ppm rated with complete combustion.

# 7 Conclusions

This study shows that the enhancement of self-dilution of confined flames can be achieved by the increase of inner diameter of the furnace. The enhancement of dilution decreases the flame temperature, and thereby, NOx emission. Thus, the increase in self-dilution in confined furnaces would lead to the reduction of NOx emission in confined flames.

# References

[1] Turns SR. (2007). Introduction to combustion: concepts and applications. McGraw-Kill (ISBN 978-007-126072-5).

[2] Li SC, Williams FA. (1999). NOx formation in two-stage methane–air flames. Combust. Flame. 118: 414.

[3] Giles DE, Som SS, Aggarwal SK. (2006). NOx emission characteristics of counter-flow syngas diffusion flames with airstream dilution. Fuel. 85: 1729.

[4] Coats CM, Richardson AP, Wang S. (2000). Non-premixed combustion in turbulent mixing layers part 2: recirculation, mixing and flame stabilization. Combust. Flame. 122: 271.

[5] Noda S, Inohae J, Nakano K, Onuma Y. (2007). An Experimental study of flame characteristics of jet diffusion flames in cylindrical furnaces. J. of Envir. Eng. 2: 505

[6] Noda S, Inohae J, Saldi ZS. (2007). NOx emission characteristics of confined jet non-premixed flames. Proc. Combust. Inst. 31: 1625.

[7] OpenFOAM: available at <http://www.openfoam.org>

[8] Menter FR. (1994). Two-equation eddy-viscosity turbulence models for engineering applications. AIAA J. 32: 1598.

[9] Golovichev V, Nordin N, Jarnicki R, Chomiak J. (2000). 3-D diesel-spray simulations using a new detailed chemistry turbulent combustion model. SAE paper. 2000-01-1891.

[10] Somarathne KDKA, Ito T, Noda S. (2012). Numerical simulation of turbulent non-premixed propane flames in a cylindrical furnace using the partially stirred reactor model. The 23rd International Symposium on Transport Phenomena, Auckland, New Zealand.

[11] Djavdan E, Darabiha N, Glovangigli V, Candel. (1991). Strained propane-air flames with detailed and reduced kinetics schemes. Combust. Sci. Tech. 76:287.

[12] Contino F, Jeaqnmart H, Lucchini T, D'Errico G. (2011). Coupling of in-situ adaptive tabulation and dynamic adaptive chemistry. Proc. Combust. Inst. 33: 3057.

[13] Hewson JC, Bollig M. (1996). Reduced mechanisms for NOx emissions from hydrocarbon diffusion flames. Proc. Combust. Inst. 26: 2171.

[14] Ju Y, Niioka T. (1997). Computation of NOx emission of a methane-air diffusion flame in a two-dimensional laminar jet with detailed chemistry. Combust. Theory and Model. 1: 243.

[15] Bowman CT, Hanson RK, Davidson DF, Gardiner WC, Lissianski V, Smith GP, Golden DM, Frenklach M.< http://www.me.berkeley.edu/gri_mech/>.